Citrate-based materials fuel human stem cells by metabonegenic regulation

Chuying Ma[a,b,c], Xinggui Tian[d,e], Jimin P. Kim[a,b,c], Denghui Xie[a,b,c,d], Xiang Ao[d,e], Dingying Shan[a,b,c], Qiaoling Lin[a,b,c], Maria R. Hudock[a,b,c], Xiaochun Bai[d,e,1], and Jian Yang[a,b,c,1]

[a]Department of Biomedical Engineering, The Pennsylvania State University, University Park, PA 16801; [b]Materials Research Institute, The Pennsylvania State University, University Park, PA 16801; [c]The Huck Institutes of the Life Sciences, The Pennsylvania State University, University Park, PA 16801; [d]Academy of Orthopedics, Guangdong Province, Guangdong Provincial Key Laboratory of Bone and Joint Degenerative Diseases, The Third Affiliated Hospital of Southern Medical University, Guangzhou 510280, China; and [e]Department of Cell Biology, School of Basic Medical Sciences, Southern Medical University, Guangzhou 510515, China

Edited by David A. Weitz, Harvard University, Cambridge, MA, and approved October 22, 2018 (received for review July 27, 2018)

A comprehensive understanding of the key microenvironmental signals regulating bone regeneration is pivotal for the effective design of bioinspired orthopedic materials. Here, we identified citrate as an osteopromotive factor and revealed its metabonegenic role in mediating citrate metabolism and its downstream effects on the osteogenic differentiation of human mesenchymal stem cells (hMSCs). Our studies show that extracellular citrate uptake through solute carrier family 13, member 5 (SLC13a5) supports osteogenic differentiation via regulation of energy-producing metabolic pathways, leading to elevated cell energy status that fuels the high metabolic demands of hMSC osteodifferentiation. We next identified citrate and phosphoserine (PSer) as a synergistic pair in polymeric design, exhibiting concerted action not only in metabonegenic potential for orthopedic regeneration but also in facile reactivity in a fluorescent system for materials tracking and imaging. We designed a citrate/phosphoserine-based photoluminescent biodegradable polymer (BPLP-PSer), which was fabricated into BPLP-PSer/hydroxyapatite composite microparticulate scaffolds that demonstrated significant improvements in bone regeneration and tissue response in rat femoral-condyle and cranial-defect models. We believe that the present study may inspire the development of new generations of biomimetic biomaterials that better recapitulate the metabolic microenvironments of stem cells to meet the dynamic needs of cellular growth, differentiation, and maturation for use in tissue engineering.

metabonegenic regulation | energy metabolism | citrate-based materials | phosphoserine | stem cells

Bone regeneration represents a substantial component of clinical practice with more than 2 million cases of bone grafting performed each year worldwide (1) for the treatment of nonunion defects, trauma-related injuries, congenital defects, and tumor excision as well as problems resulting from metabolic disorders such as obesity and diabetes mellitus. Although significant progress has been made in the development of orthopedic biomaterials, existing materials are limited by poor mimicking of the native bone and often lack the biochemical and biological coordination necessary to mediate complex bone healing (2). Thus, a deeper understanding of the microenvironmental signals involved in bone repair, including the concerted actions of growth factors, extracellular matrix (ECM) topography, and mechanical stimuli (2), could be pivotal in guiding the design of materials that encourage stem cell differentiation and bone formation to improve healing outcomes. Emerging studies have placed a spotlight on metabolic factors in the cell microenvironment of bone, including O_2 (3), glucose (4), and glutamine (5), uncovering previously neglected factors that play distinctive roles in stem cell development and differentiation. For example, metabolic factors such as glucose have been shown to regulate the energy needs of stem cells during osteoblast differentiation, whereas factors leading to an energy deficit largely impair bone formation (4). Still, a full picture of the metabolic processes guiding or supporting osteogenic differentiation is far from complete, as exemplified by the inadequate understanding of the role of citrate, an intermediary of cellular metabolism (6–8), in bone.

Citrate is a strongly bound and integral component that is crucial for native bone; over 90% of the body's total citrate content is stored in bone matrix and is released during bone resorption (9). As a key intermediate metabolite in the tricarboxylic acid (TCA) cycle, citrate also plays crucial regulatory roles in maintaining cell energy homeostasis (6, 7); therefore, citrate homeostasis must be tightly controlled. Intriguingly, recent studies have reported that the membrane transporter responsible for citrate uptake from the extracellular milieu, solute carrier family 13 member 5 (*SLC13a5*), is upregulated during early-stage osteointegration and active bone formation in response to mechanical loading (10, 11). The incorporation of citrate into biomaterials has also been found to enhance bone formation (12–14). These studies support the influence of exogenous citrate supplementation in osteogenic processes. However, a comprehensive understanding of the effect of citrate in osteodifferentiation is lacking, and the link between the role of

Significance

Differentiation of mesenchymal stem cells (MSCs) to bone-forming cells is central to bone regeneration, the extent of which is largely regulated by microenvironment factors. Here, we find that citrate as a metabolic factor that is abundant in bone can be consumed by MSCs to fuel osteogenesis by regulating metabolic pathways. We explored the mechanism of citrate benefit and designed a biomimetic citrate-based material that could provide a citrate- and phosphoserine-rich environment during degradation based on the previously unexplored concerted action between the two bioactive factors in accelerating bone regeneration. Together, these studies open up avenues for the study of stem cell biology and design of bone biomaterials to treat critically sized defects and bone disorders of metabolic origin.

Author contributions: C.M., X.T., X.B., and J.Y. designed research; C.M., X.T., J.P.K., D.X., X.A., D.S., Q.L., and M.R.H. performed research; C.M., X.T., J.P.K., D.S., X.B., and J.Y. analyzed data; and C.M., J.P.K., and J.Y. wrote the paper.

Conflict of interest statement: J.Y. and The Pennsylvania State University have a financial interest in Acuitive Technologies, Inc. These interests have been reviewed by the University's Institutional and Individual Conflict of Interest Committees and are currently being managed by the University.

This article is a PNAS Direct Submission.

[1]To whom correspondence may be addressed. Email: jxy30@psu.edu or baixc15@smu.edu.cn.

This article contains supporting information online at www.pnas.org/lookup/suppl/doi:10.1073/pnas.1813000115/-/DCSupplemental.

Published online November 26, 2018.

extracellular citrate in cellular metabolism and its eventual role in osteogenic differentiation has yet to be established.

Here, we identify this central link in which extracellular citrate, taken up through SLC13a5, mediates the metabolic regulation of cellular energy status that influences the progression of human mesenchymal stem cells (hMSCs) to an osteophenotype, an effect referred to as "metabonegenic regulation" (Fig. 1). Inspired by this breakthrough model, we designed a citrate-based orthopedic biomaterial based on the following rationale. (*i*) We identified phosphoserine (PSer), an organic phosphate donor involved in biomineralization, as an osteopromotive factor that uniquely exhibited concerted action with citrate to elevate intracellular ATP levels of hMSCs differentiating toward osteogenesis. (*ii*) Following on our previous work on the fluorescent mechanisms of biodegradable photoluminescent polymers (BPLPs) (15), we designed a facile, one-pot synthesis from citrate, PSer, and a diol to produce a brightly photoluminescent polymer that would enable both a multitude of imaging functionalities and the controlled release of the bioactive factors citrate and PSer from a biodegradable platform. (*iii*) The resulting photoluminescent biodegradable polymer, BPLP-PSer, was further fabricated into BPLP-PSer/hydroxyapatite (HA) microparticulate (MP) scaffolds exhibiting biomimetic PSer-rich bioactive surfaces for improved tissue response and early bone deposition (14, 16). Broadly, these findings may transform the current understanding of cell metabolism and energy homeostasis from being bystanders to being pivotal factors guiding osteogenic stem cell differentiation (2) and may inform the future design of biomimetic orthopedic materials.

Results

Citrate as an Osteopromotive Factor Enhances Osteophenotype Progression. We first sought to uncover the role of citrate that is released from biomaterials (12, 13) in the osteogenic differentiation of hMSCs into osteoblasts. Growth medium (GM) supplemented with exogenous citrate at different dosages (0–2,000 μM citrate, pH 7.4) showed little increase in hMSC proliferation and an absence of calcium deposition as shown by Alizarin Red staining (*SI Appendix*, Fig. S1 *A* and *B*). In contrast, citrate supplementation in osteogenic (OG) medium revealed a dose-dependent elevation of osteogenic markers (*SI Appendix*, Fig. S1 *B–E*), indicating citrate has an osteopromotive role only after osteodifferentiation is initiated. Among the citrate concentrations studied, 200 μM was identified as the optimal dosage for exogenous citrate supplementation based on alkaline phosphatase (ALP) and osteopontin (OPN) expression (*SI Appendix*, Fig. S1 *C–E*). The osteopromotive effect of citrate was confirmed by real-time PCR (Fig. 2*A*), which showed remarkably elevated expression of Runt-related transcription factor 2 (*Runx2*), the earliest master determinant of osteogenesis, as well as the genes encoding bone matrix proteins such as *Col1a1* (encoding collagen type 1 alpha 1) and *SPP1* (encoding OPN) in the 200-μM citrate treatment group compared with the OG control group after 7 and 14 d. Consistently, ELISA tests (Fig. 2*B*) showed favorable accumulation of Runx2 protein with citrate treatment as early as day 4.

Osteogenic differentiation is a three-stage process of proliferation, matrix maturation, and mineralization (Fig. 2*C*). To investigate the differentiation-stage dependence of the citrate effect, we restricted citrate (200 μM) supplementation to one of three time periods (group I: days 0–4; group II: days 4–14; and group III: days 14–21) corresponding to each stage of differentiation, plus a pretreatment period before osteoinduction (group IV). Notably, early citrate supplementation at only the proliferation stage (group I) significantly elevated ALP production at day 7 (*SI Appendix*, Fig. S1*F*), and the osteogenic effects of this early treatment were well sustained through day 14 (Fig. 2*D*). In contrast, late citrate supplementation during the mineralization stage (group III) exhibited diminished cumulative osteopromotive potential compared with the other groups as measured by total calcium/protein ratio after 21 d (Fig. 2*D*), highlighting the important role of citrate treatment at the early stages of osteogenic differentiation. Surprisingly, even citrate pretreatment in growth medium for 4 d before osteogenic induction greatly improved the downstream osteophenotype progression, as shown by increased ALP production and higher calcium/protein ratios (Fig. 2*E*). These exciting results indicated that exogenous citrate is an osteopromotive factor with a dosage dependence centered around 200 μM and timing dependence favoring supplementation at early stages.

Citrate Enhances Osteophenotype Progression Through SLC13a5. Because protein synthesis and altered metabolic activity precede and cross-talk with Runx2 expression for orchestrated osteophenotype progression in cells of osteoblast lineage (4, 5), we were excited to discover that protein synthesis increased significantly in hMSCs pretreated with citrate for 24 or 96 h compared with the respective control groups without citrate in the GM (Fig. 3*A*). The protein synthesis inhibitor cycloheximide (Chx) as a negative control and Torin 1 as an mTOR inhibitor abolished this activity, revealing the mTOR dependence of citrate-mediated protein synthesis. Given these findings, together with citrate's role as a key metabolite for regulating cell energy metabolism (6–8, 17), we proposed a metabonegenic model in which exogenous citrate mediates intracellular metabolic events in preparation for osteogenic differentiation.

To set the groundwork for testing this model, we next demonstrated that the uptake of extracellular citrate is linked to downstream osteogenic processes by identifying and validating the transport mechanism involved. First, we performed a citrate assay (*SI Appendix*, Fig. S2*A*) showing a marked increase in the intracellular citrate of hMSCs upon 24 h incubation with citrate-supplemented medium, thus affirming that exogenous citrate is indeed taken up by cells because little endogenous citrate is produced by hMSCs, which rely mostly on glycolysis. Using Western blotting, we next studied the expression of the citrate plasma membrane transporter SLC13a5 before and after osteogenesis of hMSCs. We discovered that SLC13a5 expression was greatest in undifferentiated and early-stage differentiating hMSCs, gradually decreasing after 4 d of differentiation (Fig. 3*B*). Importantly,

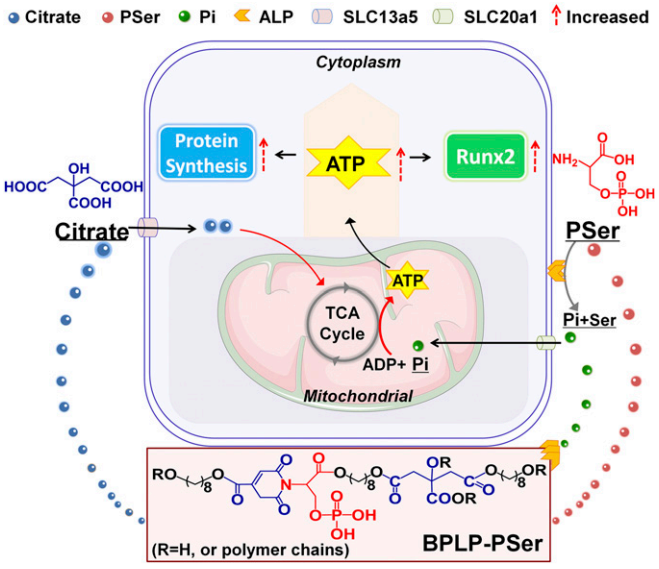

Fig. 1. Schematic model of the metabonegenic citrate-based material BPLP-PSer, which induces concerted citrate/PSer-mediated regulation of cell energy metabolism toward osteophenotype progression. Pi, inorganic phosphate.

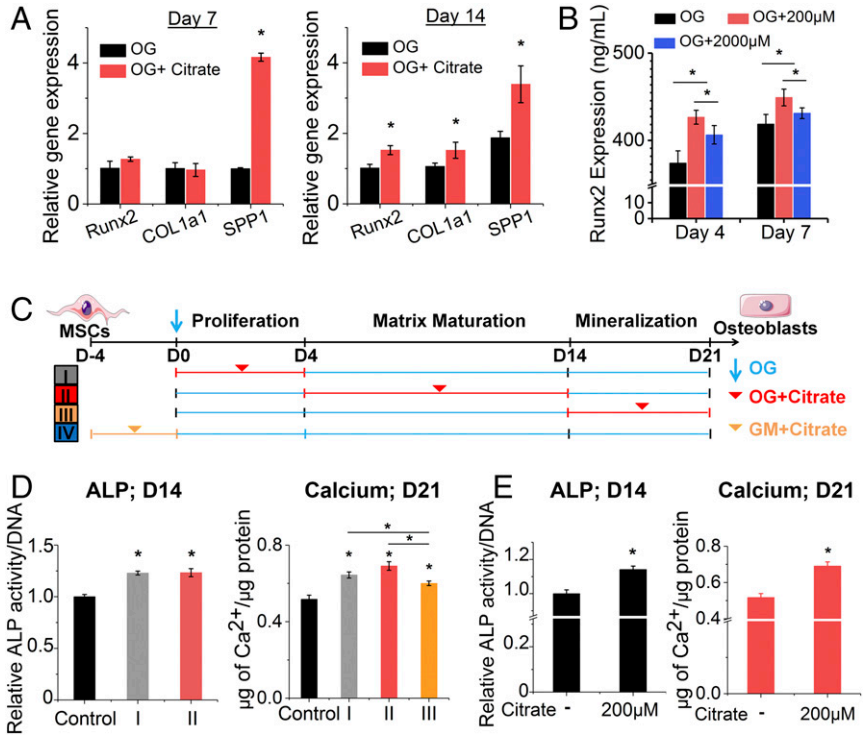

Fig. 2. The osteopromotive effect of solute citrate. (*A*) Gene expression of *Runx2*, *COL1a1*, and *SPP1* in differentiating hMSCs with/without citrate supplementation at 200 μM in established OG medium for 7 and 14 d, as determined by real-time PCR. Data are shown as the expression of target genes after normalization relative to corresponding control groups without citrate supplementation at day 7 (value set to 1.0). (*B*) Expression of Runx2 transcription factor in hMSCs with/without citrate supplementation in OG medium as determined by ELISA. In *A* and *B*, $n \geq 4$ biological replicates per group. (*C*) Schematic illustration of the experimental design studying differentiation-stage dependence by restricting citrate supplementation (200 μM) only at the proliferation stage (group I; days 0–4), the matrix maturation stage (group II; days 4–14), the mineralization stage (group III; days 14–21), or after 4 d in GM before osteoinduction (group IV; day −4 to day 0). (*D*) ALP expression at day 14 and calcium content in hMSCs at day 21 in OG medium supplemented with citrate only at specific differentiation stages (groups I, II, and III). (*E*) ALP production and calcium content in hMSCs with/without 4 d of citrate pretreatment in GM before being subjected to osteogenic differentiation in OG medium without citrate addition (group IV). In *D* and *E*, $n = 3$–5 biological replicates per group. All data are presented as mean ± SD; $^*P < 0.05$.

the addition of PF06761281, an inhibitor of SLC13a5, negated the citrate-induced elevation of ALP production (Fig. 3*C*). Together, these results show that exogenous citrate enters hMSCs through SLC13a5, affecting downstream osteophenotype progression, thus prompting us to further examine the metabolic events leading to osteogenesis.

Citrate Elevates Intracellular ATP by Metabolic Regulation. In response to osteostimulation, hMSCs undergo a metabolic switch from glycolysis to oxidative respiration to generate more ATP (18), since the production of abundant matrix proteins during bone formation involves high energy demands (5). We investigated the role of soluble citrate in hMSC energy metabolism and specifically asked whether citrate, as a metabolic regulator, affects the cell energy status by regulating primary energy-generating metabolic flux. After 24 h of citrate treatment, hMSCs exhibited elevated intracellular ATP levels (Fig. 3*D*) and an increased oxygen consumption rate (OCR) (Fig. 3*E*)—key indicators of mitochondrial respiration—accompanied by a decrease in glycolytic flux, indicating the inhibition of glycolysis (Fig. 3*F*), and reduced production of lactate (Fig. 3*G*), the end product of glycolysis. Therefore we propose that exogenous citrate facilitates the metabolic shift in hMSCs from glycolysis to oxidative respiration to induce higher intracellular ATP synthesis. Importantly, the effect of citrate on metabolic flux, i.e., elevating intracellular ATP levels, could be abolished by blocking SLC13a5 with the inhibitor PF06761281 (Fig. 3 *D*–*G*), suggesting that the regulatory effect of exogenous citrate on cell energy metabolism is also mediated by SLC13a5. Moreover, citrate treatment of hMSCs differentiated for 14 d elicited significant effects on intracellular ATP only after 4 d of treatment (*SI Appendix*, Fig. S2*B*), whereas only 1 d of treatment markedly increased hMSC mitochondrial respiration (*SI Appendix*, Fig. S2*C*), which was likewise abolished with the inhibitor PF06761281. However, the 1-d citrate treatment had no significant effect on glycolytic flux (*SI Appendix*, Fig. S2*D*). Taking these results together with our findings that citrate treatment promotes mTOR-dependent protein synthesis and favors Runx2 accumulation, we propose a previously unexplored pathway of citrate metabonegenic regulation through which exogenous citrate enters hMSCs through SLC13a5 to regulate cell energy metabolism, elevating cellular energy levels that in turn facilitate osteophenotype progression (Fig. 1).

PSer Prolongs Citrate's Osteopromotive Effect via Concerted Citrate/PSer Metabonegenic Regulation. PSer is a functional moiety that is abundant in the noncollagenous proteins (NCPs) of natural bone. Importantly, PSer is osteopromotive (19, 20) mainly by serving as an organic phosphate donor through which ALP produces inorganic phosphate, the primary substrate for ATP production (21). Therefore, to further examine the effects of PSer on the citrate-elevated cell energy status, we treated undifferentiated hMSCs with citrate, PSer, or both. The addition of PSer exerted no significant effect on the intracellular ATP levels of hMSCs with or without citrate treatment (Fig. 3*H*), indicating that PSer has no direct influence on metabonegenic processes,

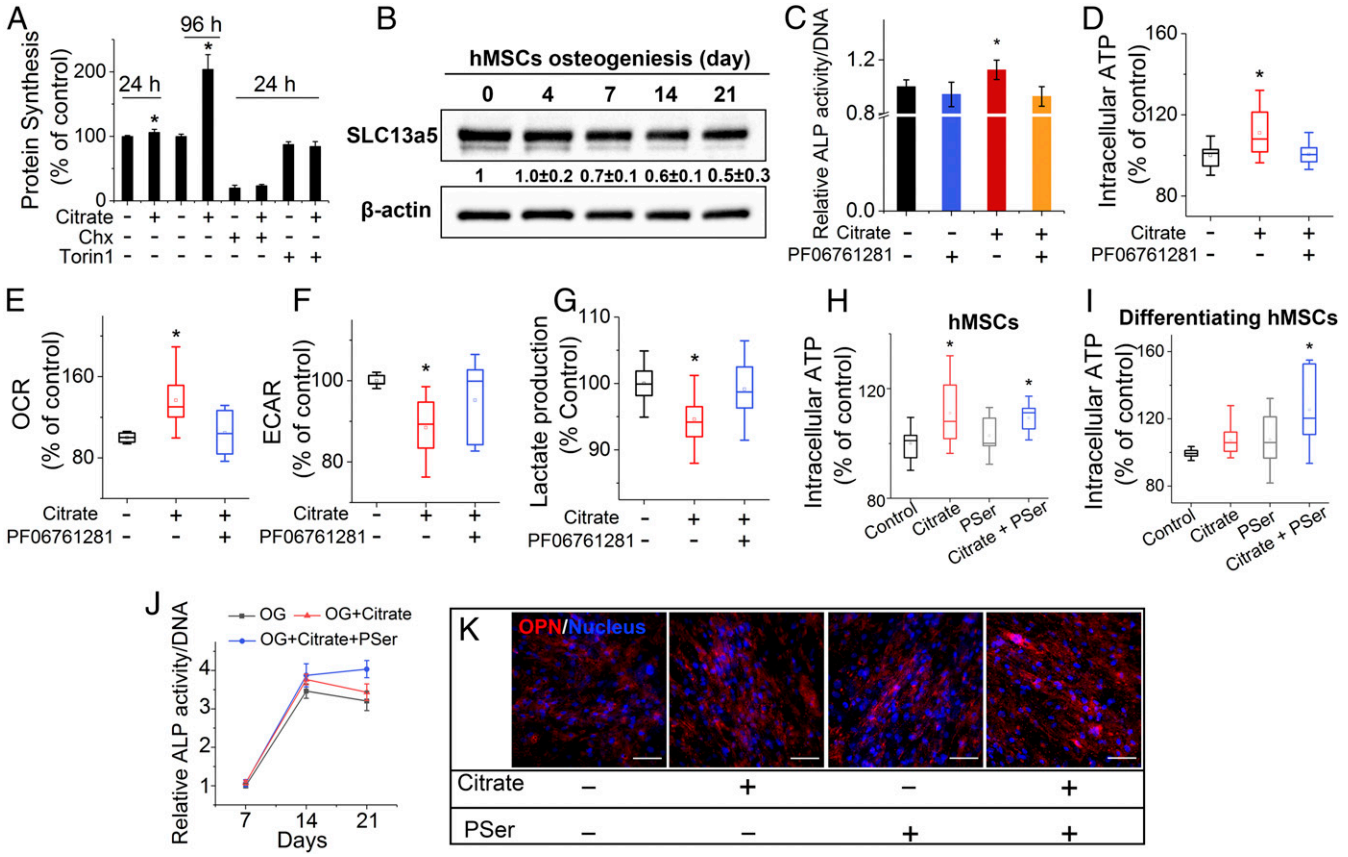

Fig. 3. Citrate metabonegenic regulation and concerted action between citrate and PSer. (*A*) Protein synthesis of hMSCs with 200 μM citrate, Chx, or Torin 1 supplementation in GM for 1 and 4 d. (*B*) Western blot of SLC13a5 expression in hMSCs during osteogenic differentiation. (*C*) ALP production of hMSCs after 14 d of differentiation in OG medium supplemented with citrate, the SLC13a5 inhibitor PF06761281, or both. In *A*–*C*, $n = 3$–5 biological replicates per group. (*D*) Intracellular ATP determination. (*E*) OCR study. (*F*) Extracellular acidification rate (ECAR) study. (*G*) Lactate production of undifferentiated hMSCs with 1 d of treatment with citrate and SLC13a5 in GM. In *D*–*G*, $n \geq 8$ biological replicates per group. (*H* and *I*) Intracellular ATP determination of hMSCs (*H*) and differentiating hMSCs (*I*) supplemented with citrate, PSer, or both in GM or OG medium, respectively. In *H* and *I*, $n = 6$–8 biological replicates per group. (*J*) ALP production of differentiating hMSCs after 7, 14, and 21 d of differentiation in OG medium supplemented with citrate or with citrate and PSer. $n = 4$ biological replicates per group; all data are presented as mean ± SD; $^*P < 0.05$. (*K*) Immunofluorescent staining of OPN (red) with DAPI nuclear counterstain (blue) expression after 21 d of differentiation in OG medium supplemented with citrate, PSer, or both. The plus (+) and minus (–) symbols denote the presence and absence, respectively, of citrate and other specific chemicals in GM/OG medium. (Scale bars: 100 μm.)

likely because the low levels of phosphatases present in undifferentiated cells render exogenous PSer biologically inactive. Specifically, ALP, expressed abundantly in osteoblasts, is known to hydrolyze soluble (22) or chemically bound PSer (23) to release inorganic phosphates. Indeed, there was a marked increase of intracellular ATP in differentiating hMSCs treated with the citrate and PSer combination, whereas individual treatments showed no difference from the OG medium control (Fig. 3*I*). Additionally, given that citric acid can react with amino acids to generate a family of citrate-based photoluminescent dyes (CPDs) (24), small-molecule citric acid-PSer (CA-PSer) was synthesized, and its effect on cell energy level was examined. There was no significant increase in the ATP level in hMSCs after 24-h treatment with CA-PSer, indicating the importance of citrate in its monomeric form for metabonegenic regulation (*SI Appendix*, Fig. S2*E*), probably because only monomeric citrate can be taken up through SLC13a5 and used for metabolic purposes.

Interestingly, the osteopromotive effects of dual treatment with citrate and PSer were particularly evident at late stages of osteogenesis, sustaining high levels of ALP (Fig. 3*J* and *SI Appendix*, Fig. S2*F*) and OPN production (Fig. 3*K*) well into day 21, whereas the ALP level dropped off in the citrate-only and control treatment groups. Even a low dosage of 40 μM PSer [lower than the reported effective dosage (19, 20)] substantially enhanced the citrate-promoted osteophenotype progression, with higher PSer dosages resulting in further elevation of ALP production (*SI Appendix*, Fig. S2*G*). These findings suggest that citrate-induced elevation of ALP levels in differentiating cells catalyzes the dephosphorylation of PSer, thereby liberating the bioactive inorganic phosphate from PSer, while exogenous PSer in turn favorably prolongs the metabonegenic effect of citrate, facilitating intracellular ATP synthesis to fuel osteophenotype progression (Fig. 1).

BPLP-PSer Is a Biodegradable Photoluminescent PSer- and Citrate-Based Polymer. This identification of concerted osteopromotive action by citrate and PSer enabled us to design bioinspired polymers in which the incorporation of PSer in citrate-based polymers may mimic the bioactive NCP-rich interface layer typically used on implant surfaces to facilitate mineral deposition and regulate bone cell activities (25, 26). To prepare BPLP-PSers, we reacted O-Phospho-DL-serine with citric acid and 1,8-octanediol via a previously described one-pot condensation reaction (15) to prepare the prepolymer, which could be further postpolymerized to generate an elastomeric cross-linked polymer network (*SI Appendix*, Fig. S3*A*). The PSer incorporation was next confirmed by ^{31}P-NMR (NMR, *SI Appendix*, Fig. S3*B*). HPLC analysis further verified the presence of PSer in both the

accelerated degradation product and the release medium of BPLP-PSer films (*SI Appendix*, Fig. S3 *C* and *D*), while phosphate assay of cross-linked films demonstrated the release of inorganic phosphate from the incorporated PSer in BPLP-PSer after ALP treatment (*SI Appendix*, Fig. S3*E*).

BPLP-PSer emitted strong fluorescence with excellent photostability (*SI Appendix*, Fig. S3 *F* and *G*), and the wavelength of the fluorescence emission was tunable by changing the excitation wavelength (Fig. 4*A*), consistent with the described previously band-shifting behavior of the dioxoprryidine (DPR) family of CPDs and BPLPs represented by CA-Ser and BPLP-Ser (15, 24), while the fluorescence intensity was tunable by changing the molar ratio of PSer (Fig. 4*B*). Similar to BPLP-Ser, the fluorescence of BPLP-PSer may be attributed to the DPR structure (15, 24) generated by a key condensation step between citrate and PSer. To demonstrate the feasibility of fluorescence tracking, we measured the gradual decay of the total fluorescence signal of BPLP-PSer films using the Maestro EX in vivo imaging system (Fig. 4*C*), which was accompanied by a corresponding increase in accumulated fluorescent signals in the degradation solution over the same (accelerated) degradation time (Fig. 4*D*). Moreover, the mass-remaining profile by conventional gravimetric analysis coincided with the remaining total fluorescence profile (Fig. 4*E*), indicating that the degradation of BPLP-PSer could be reliably tracked by either the fluorescence remaining in polymer films or the fluorescent moiety released from the polymer films over time. The mass-remaining profile of polymer degradation in accelerated (basic) conditions (*SI Appendix*, Fig. S3*H*) and in PBS (pH = 7.4) (*SI Appendix*, Fig. S3*I*) consistently revealed how the introduction of PSer impacted the degradation of the resultant polymers. BPLP-PSer films degraded more slowly than poly(octamethylene citrate) (POC) films but faster than BPLP-Ser films. As the tunable degradability of BPLPs has been demonstrated previously by varying the ratio of the monomers and the cross-linking conditions (15), BPLP-PSer may be designed to obtain the optimum degradation rate to meet the needs of specific applications.

Incorporated PSer Facilitates Mineral Deposition and Improves Cytocompatibility. To evaluate surface bioactivity for mineralization, we performed an in vitro mineralization assay by immersing cross-linked BPLP-PSer films in simulated body fluid, with poly (DL-lactide-co-glycolide) (PLGA) 75/25 as a general control along with POC and BPLP-Ser (incorporating L-serine) as citrate-based material controls. BPLP-PSer films displayed accelerated mineral deposition compared with all controls (*SI Appendix*, Fig. S4), indicating that PSer is a key monomer for facilitating mineralization in citrate-based polymer formulations. This result was further confirmed by a follow-up mineralization assay using polymer/50% HA (*SI Appendix*, Fig. S5*A*). In mechanical evaluations, the BPLP-PSer/50% HA composites possessed an impressive compressive strength of ∼200 MPa (*SI Appendix*, Fig. S5*B*), falling into the range of human cortical bone (100–230 MPa) and suggesting strong potential in orthopedic applications. BPLP-PSer also improved the maximum HA-binding capability (up to 60%) compared with BPLP-Ser (*SI Appendix*, Fig. S5*B*); notably, BPLP-PSer/60% HA improved the modulus twofold compared with the BPLP-PSer/50% HA composition.

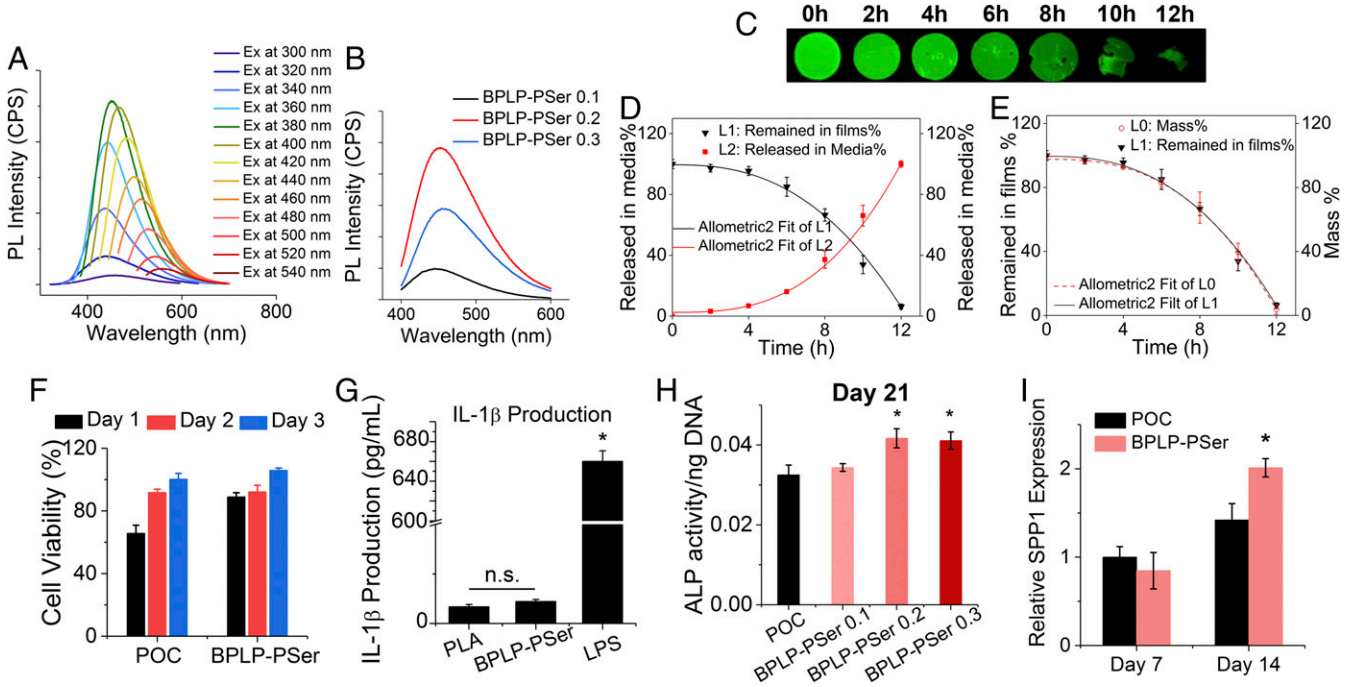

Fig. 4. BPLP-PSer as a biocompatible photoluminescent biodegradable polymer. (*A*) Emission spectra of BPLP-PSer-0.2 prepolymer displaying tunable emission wavelengths by changing the excitation wavelength. (*B*) Emission spectra of BPLP-PSer prepolymer solutions with various molar ratios of PSer excited at 370 nm. (*C*) Fluorescent images of BPLP-PSer films after accelerated degradation for a predetermined time (0, 2, 4, 6, 8, 10, or 12 h) in 0.05 M NaOH solution. (*D*) Quantitative analysis of the remaining fluorescent signal in BPLP-PSer films (L1) and the corresponding fluorescent signal in degradation medium released from polymer films (L2). (*E*) Comparison of the remaining-fluorescence profile of BPLP-PSer films (L1) with the conventional mass-remaining profile (L0). In *C*–*E*, $n = 5$ films per time point. (*F*) Cytotoxicity test on leachable extracts from polymer films. L929 cells examined by Cell Counting Kit-8 (CCK-8) show significantly greater cell viability in the BPLP-PSer group than in the POC group. (*G*) Release of inflammatory factor IL-1β from THP-1 monocytes activated by incubation with polymer films, determined by ELISA. (*H*) ALP production of differentiating hMSCs cultured in OG medium on polymer films. BPLP-PSer 0.1/0.2/0.3 indicates 0.1, 0.2, or 0.3 molar ratios of PSer to citrate. (*I*) Expression of *SPP1* encoding OPN by differentiating hMSCs cultured on polymer films in OG medium. Data are shown as the relative expression of *SPP1* after normalization to the corresponding control group without citrate supplementation at day 7 (set to 1). In *F*–*I*, $n = 3$–5 biological replicates per group. All data are presented as mean ± SD; $^*P < 0.05$; n.s., not significant.

The cytocompatibility of BPLP-PSer was systematically evaluated on leachable extracts (Fig. 4*F*) and degradation products (*SI Appendix*, Fig. S6*A*) and by direct contact on films (*SI Appendix*, Fig. S6*B*), demonstrating cell viabilities comparable with those of the PLGA control. ELISA studies further showed that the release of the inflammatory factor IL-1β from THP-1 monocytes induced by BPLP-PSer films was equivalent to that induced by the polylactic acid (PLA) control (Fig. 4*G* and *SI Appendix*, Fig. S6*C*). Furthermore, BPLP-PSer film compositions with varying PSer content (0.1–0.3 molar ratios to citrate) were all shown to support hMSC proliferation (*SI Appendix*, Fig. S6*D*) and osteogenic differentiation, with the BPLP-PSer-0.2 and BPLP-PSer-0.3 compositions significantly elevating ALP production by day 21 (Fig. 4*H* and *SI Appendix*, Fig. S6*E*) and BPLP-PSer 0.2 exhibiting significantly higher OPN gene expression by day 14 (Fig. 4*I*) than its POC counterpart.

BPLP-PSer/HA Microparticles with Ridge-and-Cliff Surface Features Support hMSC Adhesion and Proliferation. To translate the concerted osteopromotive actions of citrate and PSer into a biomimetic material for orthopedic applications, we developed a composite MP scaffold from a porous BPLP-PSer/50% HA scaffold (150- to 250-μm pore size by salt leaching) (*SI Appendix*, Fig. S7*A*) ground and sieved into 250- to 425-μm microparticles (Fig. 5*A*). The procedure was repeated for the POC/50% HA control, although the PLGA/HA control could only incorporate up to 30% of HA for MP preparation. The BPLP-PSer/HA MPs demonstrated excellent handling ability, mixing easily with saline solution (*SI Appendix*, Fig. S7 *B* and *C*), sodium hyaluronate carrier (*SI Appendix*, Fig. S7*D*), or blood from patients to facilitate surgical applications. The resulting BPLP-PSer/HA MPs greatly supported hMSC adhesion as examined by SEM, revealing that cells adhered abundantly to the cliff and ridge as well as to the groove structures(*SI Appendix*, Fig. S7 *E* and *F*) of MPs after 6 h of continuous mixing of MPs and suspended hMSCs. In addition, BPLP-PSer/HA MPs supported immediate and earlier proliferation of hMSCs compared with POC/HA MPs (*SI Appendix*, Fig. S7*G*). More importantly, hMSCs cultured on POC/HA and BPLP-PSer/HA for 4 d showed a substantial increase in intracellular ATP, almost twice that of PLGA/HA MPs (Fig. 5*B*), likely due to innate citrate metabonegenic regulation in both citrate-based MPs, whereas PSer incorporation did not provide additional benefits to undifferentiated hMSCs, as expected.

BPLP-PSer/HA MPs Promotes hMSC Differentiation. We further examined whether citrate- and PSer-presenting MPs could exert concerted action on osteogenic progression by employing 3D Transwells (pore size: 3 μm) as an in vitro cavity-defect model into which different MP formulations were inserted and cultured with hMSCs. Notably, even in the absence of osteogenic inducers, hMSCs in GM showed significantly higher ALP expression in the BPLP-PSer/HA group than in the POC/HA group (Fig. 5*C* and *SI Appendix*, Fig. S7*H*). In OG medium hMSCs in the BPLP-PSer/HA MP group displayed a substantial elevation of ALP expression by day 21 (Fig. 5*D*), outperforming those in the PLGA control group and even those in the citrate-only POC control group, supporting the notion that citrate and PSer may collaborate to elicit sustained bone-forming activities. Of note, as osteodifferentiation progressed, the MPs were integrated by cells to form fluorescent bone-like tissue constructs (Fig. 5*F* and *SI Appendix*, Fig. S8*A*) that remained intact upon compression and recovered upon unloading (Movie S1) and that had increased compressive strength and modulus (Fig. 5*E* and *SI Appendix*, Fig. S8*B*). By designing polydimethylsiloxane (PDMS) culture wells in the shape of the letters P, S, and U, we succeeded in generating P-, S-, and U-shaped fluorescent constructs (Fig. 5*F*), demonstrating the attractive potential of MPs to fill and bridge irregular defects. In fact, SEM revealed a thick layer of cells covering MP surfaces and bridging together adjacent MPs (*SI Appendix*, Fig.

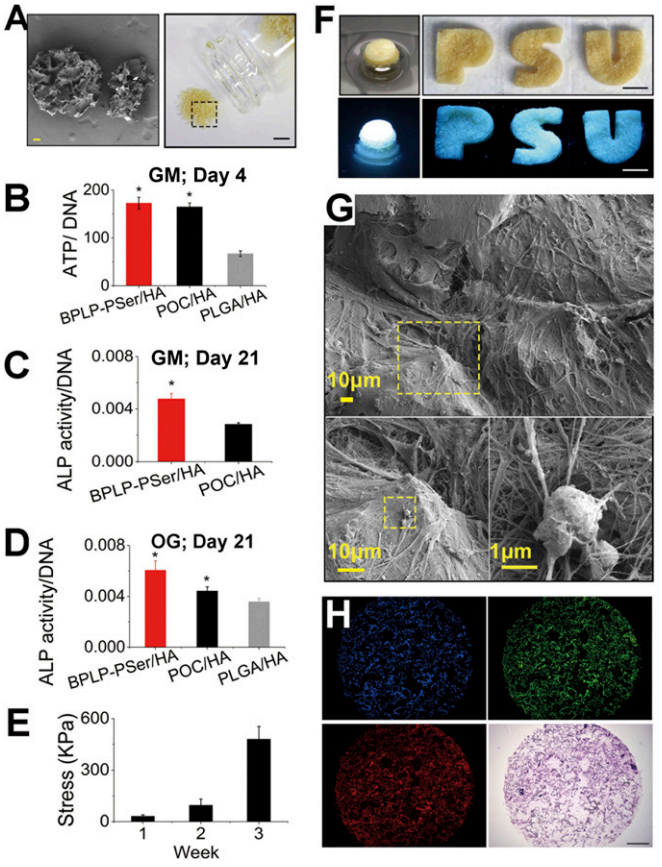

Fig. 5. BPLP-PSer/HA MP scaffolds promote hMSC differentiation. (*A*) Photographic (*Right*) and SEM (*Left*) images of BPLP-PSer/HA MP scaffolds. (Scale bars: *Right*, 5 mm; *Left*, 100 μm.) (*B*) Intracellular ATP levels (normalized to DNA) of hMSCs cultured on different MPs in GM for 4 d. $n \geq 8$ biological replicates per group. (*C* and *D*) ALP production of hMSCs in GM without osteogenic inducers cultured on MPs in Transwell 3D models (*C*) and differentiated in OG medium for 21 d (*D*). $n = 3$–5 biological replicates per group. (*E*) Compressive strength of round disk-shaped cell–MP constructs after cells differentiated for 1, 2, or 3 wk in OG medium. $n = 3$ cell–MP constructs per time point. All data are presented as mean ± SD; $^*P < 0.05$. (*F*) Photographic and fluorescent images of hMSC–MP constructs obtained with 21 d of culture in round Transwells (*Left*) or from in PDMS wells with permeable bottoms cast from 3D-printed letter molds in the shape of the letters P, S, and U (*Right*). (Scale bars: 5 mm.) (*G*) SEM images of the thick cell layer covering and bridging MPs (*Upper*) and the extensive interwoven ECM network (*Lower Left*) produced by hMSCs differentiated for 21 d in OG medium to enable mineral formation (*Lower Right*). (*H*) Fluorescent images (blue, green, and red channels) (*Upper Left*, *Upper Right*, and *Lower Left*, respectively) and H&E staining (*Lower Right*) of the cell–MP construct sections obtained by cryo-sectioning. (Scale bar: 1 mm.)

S8*C*) along with extensive ECM production forming intertwined networks that was accompanied by significant calcium phosphate mineral deposition (Fig. 5*G* and *SI Appendix*, Fig. S8*D*). Further, cryosectioning and H&E staining of the rounded bone-like disks revealed a homogeneous distribution of cells throughout the constructs (Fig. 5*H*) so that cells and MP interfaces were closely integrated (*SI Appendix*, Fig. S8*E*). Meanwhile, fluorescent imaging of the sections showed strong fluorescence from MPs at different excitation wavelengths, which also confirmed a highly porous framework generated by packed MPs in the Transwell (Fig. 5*H*) that was beneficial for cell interaction and tissue penetration.

Efficacy of BPLP-PSer/HA MPs in the Femoral Condyle-Defect Model. Next, to evaluate in vivo efficacy in promoting bone regeneration, we implanted BPLP-PSer/HA MPs into a rat femoral-condyle

defect, a standardized unicortical defect widely used for screening particulate implants (27); POC/HA MPs, PLGA/HA MPs, and no-implant groups served as comparisons. Microcomputed tomography (micro-CT) analyses at 1 and 3 mo showed more new bone formation in the BPLP-PSer/HA group at the margin of defects, resulting in decreased defect sizes compared with the POC/HA and PLGA/HA groups (Fig. 6*A* and *SI Appendix*, Fig. S9*A*). Additionally, growth of bone islands could be observed within the defects of both the BPLP-PSer/HA and POC/HA groups, while very few isolated bone islands formed in the PLGA/HA group. Of note, new bone formation was enhanced on BPLP-PSer/HA MPs compared with POC/HA MPs, as assessed by island size and number, which was confirmed by quantitative bone mineral density (BMD) analysis (*SI Appendix*, Fig. S9*A*).

H&E staining further revealed that at 1 mo new bone began to be directly deposited onto BPLP-PSer/HA MPs, while minimal bone formation was visible on other groups (Fig. 6*B*). With longer implantation, enough bone filled the intraparticulate and interparticulate spaces in the BPLP-PSer/HA and POC/HA groups to bridge adjacent MPs. In contrast, in the PLGA/HA group, fibrous tissue was found between the newly formed bone and the remnant materials, likely due to rapid degradation of the implant, and only fibrous tissue was observed in the negative control group (*SI Appendix*, Fig. S9*B*). Masson's trichrome staining showed substantially more matured bone gathered along the MP material surface and extending outward in the BPLP-PSer/HA group than in the POC/HA and PLGA-HA groups. Moreover, the fluorescence emitted from BPLP-PSer/HA MPs in tissue sections provided strong contrast between the MPs and surrounding tissue (*SI Appendix*, Fig. S9*C*), providing a facile method for analyzing the materials remaining after a predetermined time post implantation. Densitometry showed a decrease in the surface areas of MP sections with the healing time, especially after 2 mo of implantation, coinciding with the total remained-fluorescence profile (Fig. 6*C*).

BPLP-PSer/HA MPs Efficacy in a Critical-Sized Cranial-Defect Model. Our results described above demonstrated that BPLP-PSer/HA MPs can elicit faster bone formation and maturation in the

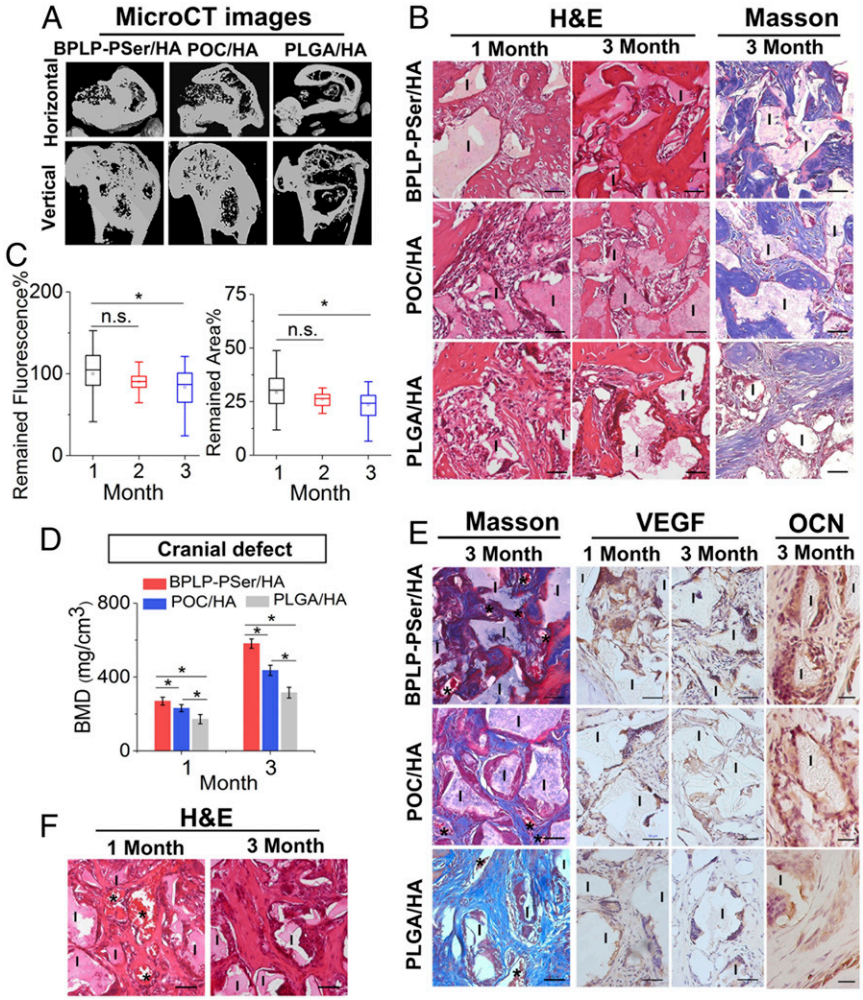

Fig. 6. In vivo efficacy of the BPLP-PSer/HA MP scaffolds. (*A*) MicroCT images of femoral-condyle defects with BPLP-PSer/HA, POC/HA, and PLGA/HA MP scaffolds at 3 mo after implantation. (*B*) H&E staining (*Left*) and Masson's trichrome staining (*Right*) of femoral-condyle defects treated with different MPs. (Scale bars: 50 μm.) I, implants. (*C*) Fluorescent analysis of remaining total fluorescent signal (*Left*) and remaining scaffold area (*Right*) in defects, determined by analyzing the fluorescent images of tissue sections in the BPLP-PSer/HA group using ImageJ (NIH). $n \geq 40$ per time point. All data are presented as mean ± SD; $^*P < 0.05$; n.s., not significant. (*D*) MicroCT BMD analysis of cranial defects with BPLP-PSer/HA, POC/HA, and PLGA/HA MPs at 3 mo after implantation. $n = 5$ defects per group. (*E*, *Left*) Masson staining. (Scale bars: 50 μm.) (*Center* and *Right*) Immunohistochemical staining of cranial defects treated with different MPs for VEGF (*Center*) and OCN (*Right*). (Scale bars: *Center*, 50 μm; *Right*, 20 μm.) (*F*) H&E staining of cranial defects treated with BPLP-PSer/HA MPs with infiltrated blood vessels. Asterisks indicate blood vessels; I, implant. (Scale bars: 50 μm.)

femoral condyle-defect model, so that our MPs can bridge nonunion defects of endochondral origin even in the absence of exogenous cell sources and growth factors. Still, defect size and location are major determinants that affect the innate capacity for bone healing (28). In particular, craniofacial bone of intramembranous origin suffers from reduced healing responses due to a poor blood supply and relative deficiency of bone marrow sources (29, 30). Therefore, we performed a second in vivo study to evaluate the potential application of BPLP-PSer/HA MPs in rat critical-sized full-thickness cranial defects, considered a severe test for bone implants.

Quantitative micro-CT analysis of BMD revealed the superior in vivo performance of BPLP-PSer/HA over other groups. Meanwhile, histomorphometric analysis at 3 mo showed more woven bone (*SI Appendix*, Fig. S10*A*) and increased red-stained mature bone generated in the BPLP-PSer/HA group than in other groups (Fig. 6*E*). In contrast, the negative control defects were filled with loose fibrous connective tissue (*SI Appendix*, Fig. S10*B*). Immunohistochemical staining consistently revealed remarkably higher VEGF expression in peri-implant cells on BPLP-PSer/HA MPs than on MPs in the control groups (Fig. 6*E*), suggesting higher blood vessel-forming activity since VEGF-producing cells in bone could largely stimulate the formation of new blood vessels. More new blood vessels were found in the BPLP-PSer/HA group, especially at 1 mo (Fig. 6*F* and *SI Appendix*, Fig. S10*C*), with the presence of red blood cells indicating the vessels' functional connection to the surrounding circulation. Also, osteocalcin (OCN) staining revealed notably higher bone matrix-formation activity in peri-implant cells around BPLP-PSer/HA MPs. Collectively, both the femoral-condyle and the cranial-defect models confirmed that BPLP-PSer/HA MPs elicited faster and superior bone formation and osteointegration in defects; new bone formation and maturation found along the material surface indicated the extensive influence of the concerted action of citrate and PSer in fueling bone regeneration.

Discussion

The impressive in vivo performances of existing citrate-presenting materials in bone regeneration, demonstrated through numerous animal models (12, 13, 31–33), motivated us to investigate the biological mechanism of citrate action on bone development. The present study has identified citrate as an osteopromotive factor; specifically, its beneficial effects are mediated by SLC13a5, the plasma membrane transporter responsible for citrate uptake. Although citrate uptake has known to regulate cell energy homeostasis (17, 34), the link between the role of extracellular citrate in osteoblast metabolism and its eventual role in osteogenic differentiation has remained elusive. Here, we identify metabonegenic regulation, a previously unexplored central link in which citrate uptake mediates the metabolic regulation of cellular energy status that influences the osteophenotype progression of hMSCs, as the central mechanism underlying citrate-promoted osteodifferentiation.

Our findings support the involvement of SLC13a5 in the beneficial effects of citrate. We demonstrated the expression of SLC13a5 in hMSCs, further showing that citrate-elevated ALP expression was dependent on SLC13a5. These findings have significant implications in bone stem cell biology, providing a biological mechanism underlying the reported contribution of exogenous citrate in teeth and bone showing that SLC13a5 deficiency in mice leads to impaired bone formation and defective tooth development (35). Similarly, consumption of extracellular citrate has been found in cancer cells that are known to be metabolically active to meet their high energetic and synthetic needs. For example, the uptake of citrate from extracellular space is required by prostate cancer cells to support their advanced metastatic behavior (36). SLC13a5 inhibition in hepatocarcinoma cells has resulted in decreased ATP production and suppressed mTOR activity (34), leading to inhibited cell proliferation. Our studies further demonstrated that inhibition of SLC13a5 in hMSCs negated the citrate-mediated metabolic changes such as ATP production, highlighting the metabolic impact of citrate on bone growth. In fact, any factor that diminishes cell energy production, whether through inhibiting the uptake of glucose, glutamine (4, 5), or citrate, as demonstrated in the present study, restricting oxygen for oxidative respiration (3), or decreasing the direct substrate for ATP synthesis (e.g., inorganic phosphate) (37), may impair bone formation by inhibiting energy-consuming activities. Given that serum and bone citrate has recently been found to be markedly reduced in aged and osteoporotic patients (38) and that potassium citrate supplementation, previously considered a buffering agent for diet acid loads, sustainably improves bone mass and density, the possibility that systemically administrated citrate could contribute to elevated bone energy status and thus be a potential therapeutic method in bone diseases is worthy of further investigation.

Next, the expression pattern of SLC13a5 matched the stage-dependent effects of citrate supplementation (Fig. 3*B*), suggesting that hMSCs exhibit a higher demand for exogenous citrate during pre- and early-stage differentiation (toward Runx2 expression, protein synthesis, and so forth) when their primary energy production is via glycolysis, typically without the production of large amounts of endogenous citrate. In contrast, cell metabolism gradually shifts to oxidative phosphorylation in the later stages of osteodifferentiation, generating endogenous citrate via the TCA cycle (18, 38, 39) while binding exogenous citrate via the extracellular calcium nodules; together, these processes may account for the decreased influence of exogenous citrate on late-stage cell energy metabolism and eventually on osteodifferentiation. The metabonegenic mechanism may be worthy of future study to explore whether nutrient- or energy-sensing pathways (e.g., the mTOR and the AMPK pathways) are involved in citrate metabonegenic regulation, especially since citrate uptake increased mTOR-dependent protein synthesis and diminished the hypothalamic AMPK activity following exogenous supplementation (40). Moreover, the involvement and up-regulation of SLC13a5 rather than SLC16a1 as the lactate membrane transporter during active bone formation (10, 11, 41) highlights the advantages of citrate-based materials for orthopedic applications compared with traditional PLA-based materials.

The above findings not only contribute to a comprehensive understanding of the temporal dependence of exogenous citrate in coordinated bone formation but also provide guidance for designing materials to further improve citrate metabonegenic regulation. For example, the present study showed that the introduction of PSer as a natural organic phosphate donor uniquely complemented the metabonegenic effect of citrate, resulting in elevated intracellular ATP levels particularly in the later stages of hMSC differentiation and thus prolonging active osteogenesis. Consistently, BPLP-PSer also induced elevated ALP production in late-stage differentiating hMSCs, likely due to bioactive inorganic phosphates generated by both the incorporated PSer in the polymer (*SI Appendix*, Fig. S3*E*) and the soluble PSer released during degradation (*SI Appendix*, Fig. S3*D*). Of note, phosphate is known to enter hMSCs via a phosphate transporter to fuel osteogenesis (37) by serving as the primary substrate of F1F0-ATPase for ATP synthesis (21), which probably accounts for the proposed concerted citrate/PSer regulation of cell energy metabolism toward active osteophenotype progression, as depicted in Fig. 1. Although the primary degradation mechanism of BPLP family has been identified as a return to monomeric materials (15), soluble oligomers are also detected in the entire pool of degradation product. The PSer moiety in those oligomeric degradation products may be as effective as the soluble PSer due to the ability of ALP to release bioactive phosphate from both soluble (22) and chemically bound PSer (23), while the chemically bound citrate moiety might not be able

to participate in the metabonegenic processes (*SI Appendix*, Fig. S2*E*). Therefore, future study is required to identify each component in the degradation product pool and to understand how those oligomeric degradation products could affect osteodifferentiation, so as to obtain a full understanding of the collective regulatory role of BPLP-PSer degradation products on stem cells.

In the succession of studies described above, we designed BPLP-PSer/HA composite MP scaffolds to provide growth guidance and osteogenic benefits for accelerated bone repair. As a demonstrated scaffold modality, MP scaffolds provide abundant bioactive surfaces for cell interactions along with well-interconnected pores for fast tissue penetration (42), enabling in vitro 3D culture studies and facile in vivo applications for bone-defect filling or augmentation. More importantly, the resulting MP scaffolds are expected to provide a biomimetic citrate- (12, 13) and PSer-rich (*SI Appendix*, Fig. S3*D*) microenvironment for surrounding hMSCs during degradation. As expected, the incorporation of citrate greatly boosted cellular energy levels (Fig. 5*B*), and the further introduction of PSer led to sustained osteogenic activity of the surrounding osteoblasts (Fig. 5 *C* and *D*). This is in accordance with our in vivo results showing that significantly more new and mature bone was formed by peri-implant cells around the BPLP-PSer/HA implants in animal models of different origin, since the activity of bone-forming cells is known to greatly affect the rate and extent of bone formation (43). Of note, VEGF expression was highest on peri-implant cells surrounding the BPLP-PSer/HA implants and was accompanied by greater numbers of new blood vessels. Since extracellular citrate is known to promote angiogenesis (44), a possible synergy between PSer and citrate toward angiogenesis awaits further investigation. Moreover, BPLP-PSer represents a singular base material that can be readily tuned to match the temporal needs of osteopromotive factors at different stages of bone healing, either by optimizing material degradation for soluble citrate/PSer release or by incorporating other microenvironment factors (e.g., cells or biochemical or biophysical factors) that can coordinate with citrate metabonegenic regulation to amplify bone regrowth.

In conclusion, in this work we have attained an understanding of the effect of citrate on osteophenotype progression, revealing a previously unexplored expression pattern of the SLC13a5 citrate transporter during osteodifferentiation and a mechanism focusing on the metabolic regulation of citrate to elevate cell energy status for bone formation (i.e., citrate metabonegenic regulation). These findings not only identify citrate as a metabolic factor that is favorable for osteodifferentiation in the stem cell microenvironment but also suggest that the use of citrate should be considered in bone biomaterials design. The biomimetic BPLP-PSer/HA provided a prolonged citrate-mediated metabonegenic effect well into the late stages of differentiation, demonstrating therapeutic potential for bone injuries and particularly for bone-defect filling or augmentation. In addition to its benefits in osteodifferentiation, and because the role of cross-talk between cell metabolism and the regulation of differentiation (45), especially in stem cells and immune cells, has been increasingly appreciated, materials-mediated metabolic regulation provides a unique opportunity for the further investigation of unexplored questions. For example, could materials-derived or exogenous supplemented citrate also contribute to the regulation of other differentiation processes with high metabolic demands, such as cardiogenesis or neurogenesis? Therefore, our present finding that citrate is a central link bridging the building blocks of materials with the metabolic events in cells may have broader implications in a wide range of tissue-engineering scenarios, opening avenues in stem cell biology and future biomaterials design.

Materials and Methods

hMSC Culture and Differentiation Study. hMSCs with more than six passages were used in the present differentiation study. To assess the effect of citrate on osteogenic differentiation, cells at ∼80% confluence were treated with an established OG medium (low-glucose DMEM with 10^{-7} M dexamethasone, 0.05 mM ascorbate-2-phosphate, and 0.01 M β-glycerophosphate) supplemented with citrate (pH adjusted) at different concentrations between 20 μM and 2,000 μM to initiate differentiation and were cultured for a predetermined number of days. The differentiation study procedure is described in detail in *SI Appendix*, *Supplementary Materials and Methods*.

Protein Synthesis, ATP Measurements, and OCR and Extracellular Acidification Rate Measurements. To assess the effects of citrate on protein synthesis, undifferentiated hMSCs seeded in 96-well black-walled plates were treated with growth medium supplemented with 200 μM of citrate, Chx or Torin 1, or both. After 24 or 96 h of incubation, protein synthesis was measured using the Protein Synthesis Assay Kit (Cayman Chemical). For intracellular ATP, mitochondria respiration, and glycolytic flux studies, hMSCs and differentiating hMSCs (differentiated for 14 d) were cultured in 96-well black-walled plates with/without citrate supplementation before measurement with the Luminescent ATP Detection Assay Kit (Abcam), the Extracellular O_2 Consumption Assay (Abcam), or the Glycolysis Assay Kit (Abcam), respectively. To inhibit citrate uptake, cells were pretreated for 1 h with 2 μM PF06761281 (Sigma-Aldrich) (the inhibitor for SLC13a5) before the medium supplemented with both citrate and PF06761281 was added to the cells.

Synthesis, Characterization, and Properties of BPLP-PSer. For BPLP-PSer-0.2 synthesis, citric acid, 1,8-octanediol, and O-phospho-DL-serine at molar ratios of 1:1.2:0.2 were mixed in a round-bottomed flask. After melting at 160 °C for 20 min, the temperature was lowered to 140 °C, and the mixture was stirred continuously for another 50 min with the stirring speed lowered gradually from 800 rpm to 80 rpm to produce the BPLP-PSer prepolymer. The prepolymer was then dissolved in 1,4-dioxane and purified by precipitation in water, followed by freeze-drying and storage in brown bottles at −20 °C. The yield of BPLP-PSer synthesis is ∼86%. Next, the PSer incorporation was characterized by ^{31}P NMR analysis and HPLC (Shimadzu). The procedure is described in detail in *SI Appendix*, *Supplementary Materials and Methods*.

Preparation and Characterization of the MP Scaffold. To prepare polymer/HA microparticulate scaffolds, 1.25 g of prepolymer was first dissolved in 1,4-dioxane to prepare 30% (by weight) polymer solutions followed by mixing with 1.25 g of HA (purum p.a. ≥90%; Sigma-Aldrich) and 10 g of NaCl particles with diameters of 150–250 μm. The mixture was spread on Teflon dishes until clay-like to form thin film scaffolds. After solvent evaporation, the scaffolds were cross-linked at 80 °C for 3 d, and all salts were leached by soaking the scaffolds in water. After freeze-drying, the prepared porous scaffolds were ground and sieved to collect the MPs with sizes between 250–425 μm.

hMSC Differentiation with MP Scaffolds. To evaluate hMSC differentiation on MPs, 25 mg of MPs were sterilized and transferred into Transwell inserts (Sigma-Aldrich) placed in 24-well plates. Then hMSCs at densities of 1.3×10^5 cells per insert were seeded and mixed with MPs. After culturing in GM medium for 14 and 21 d or in OG medium for 14 and 21 d, the generated round disk-like cell–MP constructs were washed thoroughly with PBS. One portion of the constructs was lysed with RIPA buffer to generate cell lysate and was subjected to further ALP assay and DNA quantification; the other portion was carefully removed from the inserts so that photographs could be taken and their compressive mechanical properties tested or so they could be fixed with 4% paraformaldehyde for cryo-sectioning at a thickness of 25 μm followed by H&E staining and observation under a microscope.

Rat Critical-Sized Femoral Condyle and Cranial Defects. Sprague–Dawley rats (male, age 8–10 wk, weighing ∼300 g) were used for in vivo evaluation of our microparticles. All animal experiments were carried out in compliance with a protocol approved by Southern Medical University's Animal Care and Use Committee. The animals were randomly divided into four groups in which (*i*) defects were filled with BPLP-PSer/HA microparticles (BPLP-PSer/HA group); (*ii*) defects were filled with POC/HA microparticles (POC/HA group); (*iii*) defects were filled with PLGA/HA microparticles (PLGA/HA group); and (*iv*) defects were left empty as a negative control (control group). Bone defects with a diameter of 3.5 mm were drilled at both sides of lateral femoral condyles, and pit defects 5 mm in diameter were made in the skull to create critical-sized femoral condyle and cranial defect models, respectively.

The implants, after being wetted with sterile saline, were inserted into defects via press fit. After all surgical procedures, the rats were kept in cages and maintained with a regular laboratory diet. The knees and skulls were harvested after 1, 2, and 3 mo of implantation for micro-CT and histological analysis. Detailed procedures are provided in *SI Appendix, Supplementary Materials and Methods*.

Statistical Analysis. All quantitative data are presented as mean ± SD with a minimum of three independent samples. Statistical analyses were performed using Statistical Package for Social Sciences (SPSS; v.18) software, and ordinary one-way ANOVA was performed on three or more groups with the Tukey post hoc test applied within groups. A two-tailed unpaired *t* test was applied when only two groups were compared. P values < 0.05 were regarded as statistically significant.

ACKNOWLEDGMENTS. This work was supported in part by NIH Grants CA182670, EB024829, and AR072731, Cystic Fibrosis Foundation Research Grant Yang17G0, and National Natural Sciences Foundation of China Grant 31529002.

1. Laurencin C, Khan Y, El-Amin SF (2006) Bone graft substitutes. *Expert Rev Med Devices* 3:49–57.
2. Lane SW, Williams DA, Watt FM (2014) Modulating the stem cell niche for tissue regeneration. *Nat Biotechnol* 32:795–803.
3. Wise DR, et al. (2011) Hypoxia promotes isocitrate dehydrogenase-dependent carboxylation of α-ketoglutarate to citrate to support cell growth and viability. *Proc Natl Acad Sci USA* 108:19611–19616.
4. Wei J, et al. (2015) Glucose uptake and Runx2 synergize to orchestrate osteoblast differentiation and bone formation. *Cell* 161:1576–1591.
5. Karner CM, Esen E, Okunade AL, Patterson BW, Long F (2015) Increased glutamine catabolism mediates bone anabolism in response to WNT signaling. *J Clin Invest* 125:551–562.
6. Mycielska ME, Milenkovic VM, Wetzel CH, Rümmele P, Geissler EK (2015) Extracellular citrate in health and disease. *Curr Mol Med* 15:884–891.
7. Iacobazzi V, Infantino V (2014) Citrate–New functions for an old metabolite. *Biol Chem* 395:387–399.
8. Rives ML, Shaw M, Zhu B, Hinke SA, Wickenden AD (2016) State-dependent allosteric inhibition of the human SLC13A5 citrate transporter by hydroxysuccinic acids, PF-06649298 and PF-06761281. *Mol Pharmacol* 90:766–774.
9. Dickens F (1941) The citric acid content of animal tissues, with reference to its occurrence in bone and tumour. *Biochem J* 35:1011–1023.
10. Thalji G, Gretzer C, Cooper LF (2013) Comparative molecular assessment of early osseointegration in implant-adherent cells. *Bone* 52:444–453.
11. Mantila Roosa SM, Liu Y, Turner CH (2011) Gene expression patterns in bone following mechanical loading. *J Bone Miner Res* 26:100–112.
12. Tran RT, et al. (2014) Synthesis and characterization of biomimetic citrate-based biodegradable composites. *J Biomed Mater Res A* 102:2521–2532.
13. Xie D, et al. (2015) Development of injectable citrate-based bioadhesive bone implants. *J Mater Chem B Mater Biol Med* 3:387–398.
14. Schneiders W, et al. (2007) Effect of modification of hydroxyapatite/collagen composites with sodium citrate, phosphoserine, phosphoserine/RGD-peptide and calcium carbonate on bone remodelling. *Bone* 40:1048–1059.
15. Yang J, et al. (2009) Development of aliphatic biodegradable photoluminescent polymers. *Proc Natl Acad Sci USA* 106:10086–10091.
16. Reinstorf A, et al. (2004) Phosphoserine–A convenient compound for modification of calcium phosphate bone cement collagen composites. *J Mater Sci Mater Med* 15:451–455.
17. Huard K, et al. (2015) Discovery and characterization of novel inhibitors of the sodium-coupled citrate transporter (NaCT or SLC13A5). *Sci Rep* 5:17391.
18. Pattappa G, Heywood HK, de Bruijn JD, Lee DA (2011) The metabolism of human mesenchymal stem cells during proliferation and differentiation. *J Cell Physiol* 226:2562–2570.
19. Ying X, et al. (2014) Phosphoserine promotes osteogenic differentiation of human adipose stromal cells through bone morphogenetic protein signalling. *Cell Biol Int* 38:309–317.
20. Park JW, Kim YJ, Jang JH, An CH (2011) MC3T3-E1 cell differentiation and in vivo bone formation induced by phosphoserine. *Biotechnol Lett* 33:1473–1480.
21. Bose S, French S, Evans FJ, Joubert F, Balaban RS (2003) Metabolic network control of oxidative phosphorylation: Multiple roles of inorganic phosphate. *J Biol Chem* 278:39155–39165.
22. Shinozaki T, Watanabe H, Arita S, Chigira M (1995) Amino acid phosphatase activity of alkaline phosphatase. A possible role of protein phosphatase. *Eur J Biochem* 227:367–371.
23. Spoerke ED, Anthony SG, Stupp SI (2009) Enzyme directed templating of artificial bone mineral. *Adv Mater* 21:425–430.
24. Xie Z, et al. (2017) Synthesis and characterization of citrate-based fluorescent small molecules and biodegradable polymers. *Acta Biomater* 50:361–369.
25. Hartgerink JD, Beniash E, Stupp SI (2001) Self-assembly and mineralization of peptide-amphiphile nanofibers. *Science* 294:1684–1688.
26. Puleo DA, Nanci A (1999) Understanding and controlling the bone-implant interface. *Biomaterials* 20:2311–2321.
27. Coathup MJ, Cai Q, Campion C, Buckland T, Blunn GW (2013) The effect of particle size on the osteointegration of injectable silicate-substituted calcium phosphate bone substitute materials. *J Biomed Mater Res B Appl Biomater* 101:902–910.
28. Fini M, et al. (2005) The healing of confined critical size cancellous defects in the presence of silk fibroin hydrogel. *Biomaterials* 26:3527–3536.
29. Dupoirieux L, Pourquier D, Picot MC, Neves M (2001) Comparative study of three different membranes for guided bone regeneration of rat cranial defects. *Int J Oral Maxillofac Surg* 30:58–62.
30. Spicer PP, et al. (2012) Evaluation of bone regeneration using the rat critical size calvarial defect. *Nat Protoc* 7:1918–1929.
31. Sun D, et al. (2014) Citric acid-based hydroxyapatite composite scaffolds enhance calvarial regeneration. *Sci Rep* 4:6912.
32. Tang J, et al. (2015) Fast degradable citrate-based bone scaffold promotes spinal fusion. *J Mater Chem B Mater Biol Med* 3:5569–5576.
33. Guo Y, et al. (2015) Citrate-based biphasic scaffolds for the repair of large segmental bone defects. *J Biomed Mater Res A* 103:772–781.
34. Li Z, et al. (2017) Silencing of solute carrier family 13 member 5 disrupts energy homeostasis and inhibits proliferation of human hepatocarcinoma cells. *J Biol Chem* 292:13890–13901.
35. Irizarry AR, et al. (2017) Defective enamel and bone development in sodium-dependent citrate transporter (NaCT) Slc13a5 deficient mice. *PLoS One* 12:e0175465.
36. Mycielska ME, et al. (2018) Extracellular citrate affects critical elements of cancer cell metabolism and supports cancer development in vivo. *Cancer Res* 78:2513–2523.
37. Shih Y-RV, et al. (2014) Calcium phosphate-bearing matrices induce osteogenic differentiation of stem cells through adenosine signaling. *Proc Natl Acad Sci USA* 111:990–995.
38. Chen H, et al. (2018) Bone and plasma citrate is reduced in osteoporosis. *Bone* 114:189–197.
39. Fu X, et al. (2018) Runx2/Osterix and zinc uptake synergize to orchestrate osteogenic differentiation and citrate containing bone apatite formation. *Adv Sci* 5:1700755.
40. Stoppa GR, et al. (2008) Intracerebroventricular injection of citrate inhibits hypothalamic AMPK and modulates feeding behavior and peripheral insulin signaling. *J Endocrinol* 198:157–168.
41. Ferraz EP, et al. (2017) Bioactive glass-based surfaces induce differential gene expression profiling of osteoblasts. *J Biomed Mater Res A* 105:419–423.
42. Lappalainen OP, et al. (2016) Micro-CT analysis of bone healing in rabbit calvarial critical-sized defects with solid bioactive glass, tricalcium phosphate granules or autogenous bone. *J Oral Maxillofac Res* 7:e4.
43. Caetano-Lopes J, Canhão H, Fonseca JE (2007) Osteoblasts and bone formation. *Acta Reumatol Port* 32:103–110.
44. Binu S, Soumya SJ, Sudhakaran PR (2013) Metabolite control of angiogenesis: Angiogenic effect of citrate. *J Physiol Biochem* 69:383–395.
45. Agathocleous M, Harris WA (2013) Metabolism in physiological cell proliferation and differentiation. *Trends Cell Biol* 23:484–492.